Deposition of Copper Particles and Films by the Displacement of Two Immiscible Supercritical Phases and Subsequent Reaction

Jaehoon Kim,[†,||] Douglas Taylor,[‡] James DeYoung,[‡] James B. McClain,[‡] Joseph M. DeSimone,[†,§] and Ruben G. Carbonell*,[†]

Department of Chemical and Biomolecular Engineering, North Carolina State University, Raleigh, North Carolina 27606-7905, Micell Technologies, 7516 Precision Drive, Raleigh, North Carolina 27617, Department of Chemistry, University of North Carolina at Chapel Hill, Chapel Hill, North Carolina 27599-3290, and Supercritical Fluid Research Laboratory, Energy and Environment Research Division, Korea Institute of Science and Technology (KIST), 39-1 Hawolgok-dong, Seongbuk-gu, Seoul, 136-791, Korea

Received September 30, 2008. Revised Manuscript Received January 14, 2009

Copper (Cu) particles and films were produced by forming Cu(II) compound ($Cu(hfac)_2 \cdot H_2O$) films on substrates using a displacement from two immiscible supercritical phases (DISP) technique followed by reducing the copper(II) compound films in hydrogen at 200 °C. Various surfaces including native oxide of silicon (SiO_x), titanium nitride (TiN), tungsten (W), and low-*k* dielectric materials such as Coral, JSR5109, and Silox were used as substrates. The nucleation and growth behavior of the Cu DISP process was evaluated over a range of reduction times (from 5 to 60 min) and copper(II) compound concentrations (0.5−3 wt %). At short reduction periods (5−15 min) or low Cu(II) compound concentrations (∼ 0.5 wt %), Cu particles ranging from 60 to 95 nm in diameter were produced. In contrast, at long reduction periods (45−60 min) and high concentrations (∼3 wt %), continuous Cu films with 220−450 nm in thickness were deposited on the substrates. A morphology transition from particle to film was observed at medium reduction period (∼30 min) or medium concentration range (∼1 wt %). High affinity of TiN to Cu nucleation and film formation leads to more dense and smooth films than Cu films deposited under similar conditions on SiO_x. However, nucleation of Cu DISP is not very sensitive to the surface conditions of the substrates compared with Cu CVD (chemical vapor deposition). Chemical composition analysis of the Cu film on TiN and SiO_x by X-ray photoelectron spectroscopy (XPS) and secondary ion mass spectrometry (SIMS) revealed that highly pure Cu films were obtained from Cu DISP.

1. Introduction

Copper (Cu) films have been extensively investigated as substitutes for aluminum (Al)-based interconnects in microelectronic devices with the increased demand for high packing density.[1] Cu has intrinsic advantages over Al such as lower resistivity and better resistance to electromigration and stress-induced migration. Thus Cu interconnects, combined with low-*k* materials, offer better chip performance, higher reliability, and lower power consumption compared to Al interconnects in silicon-based semiconductors.[2−4] Current Cu film deposition technologies are either vacuum-based methods such as physical vapor deposition (PVD) and chemical vapor deposition (CVD),[5−7] or solution-based methods such as electroless deposition and electrodeposition.[8−12] Although highly pure Cu films can be deposited, Cu PVD is often considered to be unsuitable for Cu damascene process. This is because Cu PVD often results in poor gap filling and conformity and creation of a void when depositing high-aspect-ratio features.[13] Utilization of Cu CVD in industry is limited by the requirement of high volatility of organocopper compounds, high deposition temperature (>200 °C), possible incorporation of impurities into the film, complexity of CVD processes, and high tool cost. Although electroless deposition and electrodeposition are simpler and less expensive techniques to deposit Cu films compared to a CVD process, the incompatibility of vacuum-based tool

* Corresponding author. E-mail: ruben@ncsu.edu. Tel.: (919) 515-5118.
† North Carolina State University.
|| Korea Institute of Science and Technology.
‡ Micell Technologies.
§ University of North Carolina at Chapel Hill.

(1) Kodas, T. T.; Hampden-Smith, M. J., Eds. *The Chemistry of Metal CVD*; VCH Publisher: New York, 1994.
(2) Lin, X. W.; Pramanik, D. *Solid State Tech.* **1998**, *41*, 63.
(3) Murarka, S. P.; Gutmann, R. J.; Kaloyeros, A. E.; Lanford, W. A. *Thin Solid Films* **1993**, *236*, 257.
(4) Theis, T. N. *IBM J. Res. Dev.* **2000**, *44*, 379.
(5) Cote, D. R.; Nguyen, S. V.; Cote, W. J.; Pennington, S. L.; Stamper, A. K.; Podlesnik, D. V. *IBM J. Res. Dev.* **1995**, *39*, 837.
(6) Griffin, G. L.; Maverick, A. W., CVD of copper from Cu(II) precursors. In *The Chemistry Metal CVD*; Kodas, T. T., Hampden-Smith, M. J., Eds.; VCH Publisher: New York, 1994; p 175.
(7) Hampden-Smith, M. J.; Kodas, T. T. Chemical vapor deposition of copper from Cu(I) compounds. In *The Chemistry of Metal CVD*; Kodas, T. T., Hampden-Smith, M. J., Eds.; VCH Publisher: New York, 1994; p 239.
(8) Dubin, V. M.; ShachamDiamand, Y.; Zhao, B.; Vasudev, P. K.; Ting, C. H. *J. Electrochem. Soc.* **1997**, *144*, 898.
(9) Moffat, T. P.; Bonevich, J. E.; Huber, W. H.; Stanishevsky, A.; Kelly, D. R.; Stafford, G. R.; Josell, D. *J. Electrochem. Soc.* **2000**, *147*, 4524.
(10) Moffat, T. P.; Wheeler, D.; Edelstein, M. D.; Josell, D. *IBM J. Res. Dev.* **2005**, *49*, 19.
(11) Shachamdiamand, Y.; Dubin, V.; Angyal, M. *Thin Solid Films* **1995**, *262*, 93.
(12) Shacham-Diamond, Y. Y. *Electrochem. Solid-State Lett.* **2000**, *3*, 279.
(13) Wenzel, C.; Urbansky, N.; Klimes, W.; Siemroth, P.; Schuelke, T. *Microelectron. Eng.* **1997**, *33*, 31.

10.1021/cm802659j CCC: $40.75
Published on Web 02/13/2009

clusters and generation of environmentally harmful waste are major concerns. Recently, a supercritical carbon dioxide ($scCO_2$)-based Cu film deposition technique, chemical fluid deposition (CFD), has drawn much attention because of its unique deposition conditions and film properties.[14−16] Highly pure Cu films with good gap-filling has been attributed to the solvent power of $scCO_2$ for organocopper compounds, the gaslike transport and interfacial tension properties of $scCO_2$ and the inherent solvation of organic byproduct into the $scCO_2$, which helps to ensure high-purity films.

Cu nanoparticles have been of great interest in recent years because of their unique chemical, electronic, and optical properties and tremendous potential applications in the areas of catalysis,[17−20] thermal conducting nanofluids,[21] lubricants,[22] optoelectronic devices,[23−25] and solid oxide fuel cells for direct oxidation of hydrocarbons.[26,27] A number of different methods have been developed to prepare Cu nanoparticles. Most of the methods are solution-based chemical techniques such as chemical reduction,[28−31] radiolytic reduction,[32] sonochemical reduction,[18,33] and solvent-extraction reduction[34] of Cu salt compounds in water and/or organic solvents. In these "wet" methods, stabilizers such as capping ligands and polymers need to be introduced to the solutions to prevent colloidal Cu nanoparticles from aggregating and precipitating. The complexity of chemical ingredients (such as starting materials, reducing agents, stabilizers and solvent), contamination of Cu nanoparticles with organic stabilizers, requirement of inert gas condition and production of chemical wastes are major drawbacks of the wet chemical methods. The preparation of stabilizer-free Cu nanoparticles has been investigated with wet methods such as electrochemical deposition,[35,36] laser irradiation,[17,37,38] pyrolysis,[39] and spray pyrolysis.[40] Vacuum-based physical techniques such as evaporation,[19,20,41,42] laser ablation,[43] atomic layer deposition,[44] and ion implants[24,25,45] are more environmentally benign ways to prepare stabilizer-free Cu nanoparticles on substrates. However, complicated vacuum operation, expensive tool cost, and low throughput associated with the vacuum-based techniques limit their wide application. Furthermore, there is an inherent challenge to all of these methods to systematically deposit the formed nanoparticles on high-performance surfaces. Therefore, there are still considerable efforts underway to develop more reliable, simpler, less-solvent-intensive, and less-expensive techniques that can produce high-quality Cu nanoparticles and controllably deposit the nanoparticles on advanced surfaces for ultimate device applications.[46−48]

Recently, we have developed a new supercritical fluid-based deposition technique, deposition from displacement of two immiscible supercritical phases (DISP).[49,50] Supercritical CO_2 and supercritical helium (scHe) are transiently immiscible at mild conditions (<6500 psi and <60 °C), thus creating an interfacial boundary between the $scCO_2$ phase and the scHe phase. When a $scCO_2$ solution phase containing a desired solute is displaced with a scHe phase, the solute is precipitated and deposited on a substrate at the interfacial boundary between the $scCO_2$ solution phase and the scHe phase. It has been demonstrated that high-quality small organic molecule films such as sucrose octaacetate and macromolecule films such as poly[(2-perfluorooctyl)ethyl acrylate] can be deposited using DISP.[49,50] In this paper, we demonstrate that Cu films and Cu nanoparticles can be produced on various substrates using the DISP process and subsequent reduction technique. The substrates used in this work included native oxide of silicon (SiO_x), titanium nitride (TiN), tungsten (W) and low-k dielectric materials such as Coral, JSR5109, and Silox. This new Cu metallizatinon technique involves coating a Cu(II) compound ($Cu(hfac)_2$•

(14) Blackburn, J. M.; Long, D. P.; Cabanas, A.; Watkins, J. J. *Science* **2001**, *294*, 141.
(15) Cabanas, A.; Blackburn, J. M.; Watkins, J. J. *Microelectron. Eng.* **2002**, *64*, 53.
(16) Ohde, H.; Kramer, S.; Moore, S.; Wai, C. M. *Chem. Mater.* **2004**, *16*, 4028.
(17) Chen, T. Y.; Chen, S. F.; Sheu, H. S.; Yeh, C. S. *J. Phys. Chem. B* **2002**, *106*, 9717.
(18) Dhas, N. A.; Raj, C. P.; Gedanken, A. *Chem. Mater.* **1998**, *10*, 1446.
(19) Varazo, K.; Parsons, F. W.; Ma, S.; Chen, D. A. *J. Phys. Chem. B* **2004**, *108*, 18274.
(20) Vitulli, G.; Bernini, M.; Bertozzi, S.; Pitzalis, E.; Salvadori, P.; Coluccia, S.; Martra, G. *Chem. Mater.* **2002**, *14*, 1183.
(21) Eastman, J. A.; Choi, S. U. S.; Li, S.; Yu, W.; Thompson, L. J. *Appl. Phys. Lett.* **2001**, *78*, 718.
(22) Liu, G.; Li, X.; Qin, B.; Xing, D.; Guo, Y.; Fan, R. *Tribol. Lett.* **2004**, *17*, 961.
(23) Savoini, B.; Caceres, D.; Gonzalez, R.; Chen, Y.; Pinto, J. V.; da Silva, R. C.; Alves, E. *Nucl. Instrum. Methods Phys. Res., Sect. B* **2004**, *218*, 148.
(24) Stepanov, A. L.; Popok, V. N.; Hole, D. E.; Khaibullin, I. B. *Appl. Phys. A: Mater. Sci. Process.* **2002**, *74*, 441.
(25) Townsend, P. D.; Brooks, R.; Hole, D. E.; Wu, Z.; Turkler, A.; Can, N.; Suarez-Garcia, A.; Gonzalo, J. *Appl. Phys. B: Lasers Opt.* **2001**, *73*, 345.
(26) Gorte, R. J.; Park, S.; Vohs, J. M.; Wang, C. H. *Adv. Mater.* **2000**, *12*, 1465.
(27) Park, S. D.; Vohs, J. M.; Gorte, R. J. *Nature* **2000**, *404*, 265.
(28) Huang, H. H.; Yan, F. Q.; Kek, Y. M.; Chew, C. H.; Xu, G. Q.; Ji, W.; Oh, P. S.; Tang, S. H. *Langmuir* **1997**, *13*, 172.
(29) Pileni, M. P. *Langmuir* **1997**, *13*, 3266.
(30) Suryanarayanan, R.; Frey, C. A.; Sastry, S. M. L.; Waller, B. E.; Bates, S. E.; Buhro, W. E. *J. Mater. Res.* **1996**, *11*, 439.
(31) Wang, H. Y.; Huang, Y. G.; Tan, Z.; Hu, X. Y. *Anal. Chim. Acta* **2004**, *526*, 13.
(32) Henglein, A. *J. Phys. Chem. B* **2000**, *104*, 1206.
(33) Salkar, R. A.; Jeevanandam, P.; Kataby, G.; Aruna, S. T.; Koltypin, Y.; Palchik, O.; Gedanken, A. *J. Phys. Chem. B* **2000**, *104*, 893.
(34) Song, X. Y.; Sun, S. X.; Zhang, W. M.; Yin, Z. L. *J. Colloid Interface Sci.* **2004**, *273*, 463.
(35) Bandyopadhyay, S.; Chakravorty, D. *J. Mater. Res.* **1997**, *12*, 2719.
(36) Zhou, X. J.; Harmer, A. J.; Heinig, N. F.; Leung, K. T. *Langmuir* **2004**, *20*, 5109.
(37) Yeh, M. S.; Yang, Y. S.; Lee, Y. P.; Lee, H. F.; Yeh, Y. H.; Yeh, C. S. *J. Phys. Chem. B* **1999**, *103*, 6851.
(38) Yeh, Y. H.; Yeh, M. S.; Lee, Y. P.; Yeh, C. S. *Chem. Lett.* **1998**, 1183.
(39) Hambrock, J.; Becker, R.; Birkner, A.; Weiss, J.; Fischer, R. A. *Chem. Comm.* **2002**, 68.
(40) Kim, J. H.; Germer, T. A.; Mulholland, G. W.; Ehrman, S. H. *Adv. Mater.* **2002**, *14*, 518.
(41) Palasantzas, G.; Koch, S. A.; De Hosson, J. T. M. *Appl. Phys. Lett.* **2002**, *81*, 1089.
(42) Ponce, A. A.; Klabunde, K. J. *J. Mol. Catal. A: Chem.* **2005**, *225*, 1.
(43) Paszti, Z.; Peto, G.; Horvath, Z. E.; Karacs, A.; Guczi, L. *J. Phys. Chem. B* **1997**, *101*, 2109.
(44) Johansson, A.; Torndahl, T.; Ottosson, L. M.; Boman, M.; Carlsson, J. O. *Mater. Sci. Eng., C* **2003**, *23*, 823.
(45) Takeda, Y.; Lu, J.; Plaksin, O. A.; Amekura, H.; Kono, K.; Kishimoto, N. *Nucl. Instrum. Methods Phys. Res., Sect. B* **2004**, *219−20*, 737.
(46) Chen, P.; Wu, X.; Lin, J.; Tan, K. L. *J. Phys. Chem. B* **1999**, *103*, 4559.
(47) Li, C. M.; Lei, H.; Tang, Y. J.; Luo, J. S.; Liu, W.; Chen, Z. M. *Nanotechnology* **2004**, *15*, 1866.
(48) Xie, S. Y.; Ma, Z. J.; Wang, C. F.; Lin, S. C.; Jiang, Z. Y.; Huang, R. B.; Zheng, L. S. *J. Solid State Chem.* **2004**, *177*, 3743.
(49) Kim, J.; Carbonell, R. G. *Lamgmiur* **2006**, *22*, 2117.
(50) Kim, J.; McClain, J. B.; Carbonell, R. G. *J. Supercrit. Fluids* **2007**, *43*, 139.

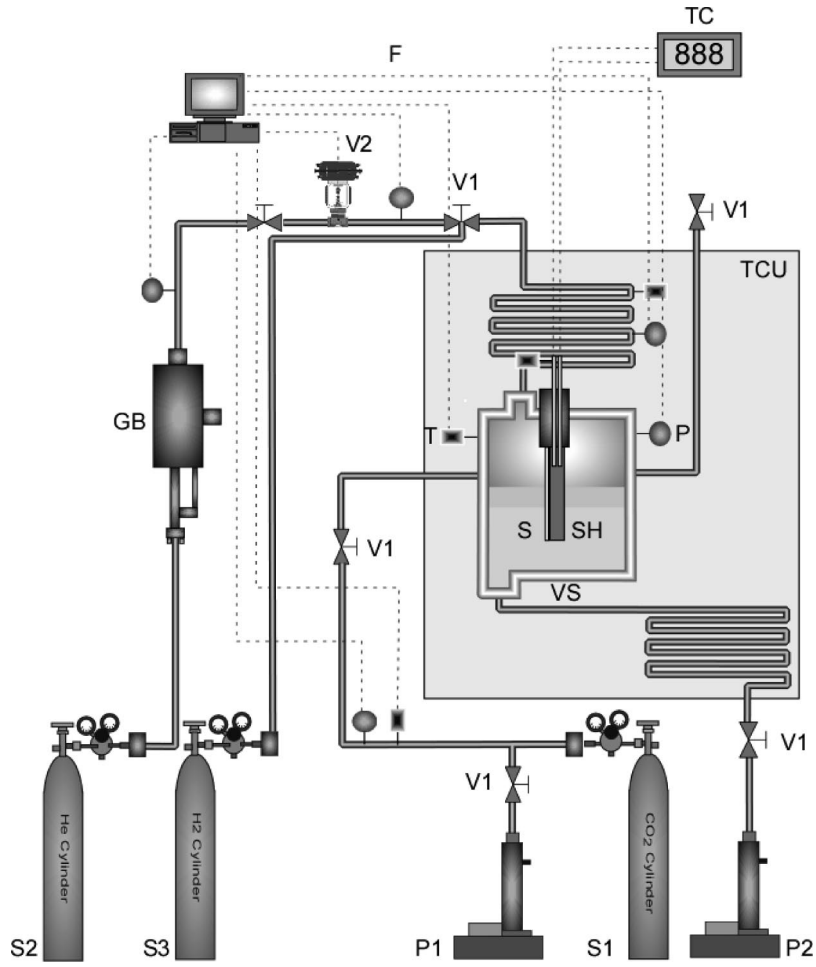

Figure 1. Schematic of the deposition from displacement of two immiscible supercritical phases (DISP) apparatus. VS, high-pressure coating vessel; V1, Isolation valves; V2, pneumatic flow control valve; S1, CO_2 source tank; P1, ISCO syringe pump at the CO_2 source; S2, He source tank; GB, gas booster; P2, ISCO syringe pump at the downstream; F, feedback control loop; P, pressure transducer; T, thermocouple; TC, substrate heating stage temperature controller; TCU, coating vessel temperature control unit.

H_2O or Cu(I/II) hexafluropentanedionate−vinyltrimethylsilane) on the substrates from DISP followed by reduction in hydrogen (H_2) at a temperature of 200 °C. The sections that follow describe the DISP apparatus and process, the effects of reduction period and $Cu(hfac)_2 \cdot H_2O$ solution concentration on particle size, film thickness and morphology as determined by scanning electron microscopy (SEM). The effects of the variable surface properties of the substrates on initial nucleation and growth behavior and final film morphology will be discussed. The chemical composition of Cu films characterized by X-ray photoelectron spectroscopy (XPS) and secondary ion mass spectrometry (SIMS) will be discussed. The texture of Cu films measured by X-ray diffraction (XRD) will be also discussed.

2. Experimental Section

2.1. Materials. Cu (II) hexafluoroacetylacetonate hydrate ($Cu(hfac)_2 \cdot H_2O$), Cu (I /II) hexafluoropentanedionate-vinyltrimethylsilane, acetone (purity of 99.9%) and methanol (purity of 99.9%) were purchased from Sigma-Aldrich (St. Louis, MO) and used as received. Type ⟨100⟩ silicon wafer with 20.6 Å (±0.8 Å) thick native oxide layer was purchased from Silicon Valley Microelectronics, Inc. (San Jose, CA). 500Å TiN/5000Å thermal silicon oxide/Si, 5000Å W/400Å TiN/250Å Ti/6300Å thermal silicon oxide/Si, and 10000Å Silox/thermal oxide/Si were purchased from International Sematech (Austin, TX). 2000Å Coral/Si was provided by SEZ group (Zurich, Switzerland). 2000Å JSR5109/Si was obtained by Lam Research Corporation (Fremont, CA). The substrates were cut to coupons with a size of 1 cm × 5 cm. The CO_2 source was Coleman grade (purity of 99.99%) and the He and H_2 sources were Ultra High Purity (purity of 99.999%) obtained from National Welders (Charlotte, NC).

2.2. Deposition from Displacement of Two Immiscible Supercritical Phases (DISP) Apparatus. Deposition experiments were carried out in a cold-wall type high-pressure reactor. A schematic of a deposition from displacement of two immiscible supercritical phases (DISP) apparatus is shown in Figure 1. The apparatus consists of a coating vessel (VS), a pneumatic flow control valve (V2), an air-driven gas booster compressor (GB), a CO_2 inlet ISCO pump (P1), a downstream ISCO pump (P2), isolation valves (V1), a computer control system (F), a substrate heating stage (SH), a substrate heating stage temperature controller (TC), and a temperature control unit (TCU) for the coating vessel. The coating vessel (VS) is cylindrical in shape with an inside diameter of 1.75 cm and an inside height of 7.61 cm, giving a volume of 18.3 mL. The vessel is equipped with a sapphire window and a window screw cap at the bottom for visual inspection of the coating solution. At the top of the coating vessel, a sealing gland fixed to a screw cap was used for electrical feedthrough to the inside of the coating vessel. A model PL-18-A4(2CU/1J)-G sealing gland was purchased from Conax Buffalo Technologies (Buffalo, NY). Four solid conductor wires (two copper wires for a cartridge heater and two

J type thermocouple calibration type wires for a thermocouple) with Kapton insulation are sealed individually inside of the sealing gland. The pressure of the sealing gland is rated up to 10,000 psi at 20 °C and the temperature is rated from −240 to 232 °C. The coating vessel and the screw caps were manufactured at the North Carolina State University Instrumentation Shop.

The substrate temperature and the coating vessel wall temperature were controlled individually. For the control of the substrate temperature, an aluminum heating stage was used. A heater and a thermocouple were inserted in the aluminum heating stage. The heater is an electrical cartridge type with 0.32 cm in diameter and 5.1 cm in length and the thermocouple was a J type with the same dimensions as the cartridge heater. The heater and the thermocouple were connected to the conductor wires inserted into the sealing gland. The model C2A5-E12 cartridge heater and the model 20CJFGD012A thermocouple were manufactured by Watlow (St. Louis, MI). The aluminum heating stage is rectangular in shape with dimension of 5.5 cm × 1.5 cm × 0.5 cm and it has two separate holes with 0.32 cm in diameter for the insertion of the heater and the thermocouple. The substrate at each deposition run was fixed to the heating stage using a 1 cm long metal clamp. The aluminum heating stage was manufactured at the North Carolina State University Instrumentation Shop. The temperature of the aluminum heating stage was controlled using a model SD6C-ACAA-AARG temperature PID controller purchased from Watlow (St. Louis, MI).

The temperature of the coating vessel wall was controlled by housing the coating vessel including tubings at the inlet and outlet of the coating vessel in a model 4EM mechanical convection incubator (TCU) manufactured at Precision Scientific (Winchester, VA). The upstream scHe temperature was controlled by flowing scHe to a 15 m long tubing with a preheating unit that was connected to the top port of the coating vessel. The downstream $scCO_2$ solution temperature was controlled by connecting a 10 m long tubing to the bottom port of the coating vessel. The temperature changes were monitored using type K thermocouples (T) from Omega Engineering, Inc. The temperature of the ISCO pump at the downstream line was controlled by circulating silicon oil to a heating/cooling jacket around a cylinder of the ISCO pump using a model EX-7 Bath/Circulator manufactured by Thermo NESLAB (Newington NH). The temperature of the coating vessel, the upstream scHe line, and the downstream $scCO_2$ solution line can be maintained within ± 0.1 °C during coating.

The upstream scHe pressure was controlled by using the air-driven gas booster compressor (GB) and the pneumatic flow control valve (V2). The model AG-152 gas booster was manufactured at Haskel International, Inc. (Burbank, CA). A gas barrel section of the gas booster is capable of withstanding pressures up to 20,000 psi and temperatures up to 115 °C. The scHe pressure at the outlet of the gas barrel was controlled by a constant airflow to an air-driven section of the gas booster. The inlet air pressure to the air-driven section is controlled by using a Fairchild Model 10 Pneumatic Precision Regulator (Winston-Salem, NC) with a model PX303−200G5V Omega Engineering (Stamford, CT) pressure transducer. For more precise control of the upstream scHe pressure, a type 766 Research Control Valve (model 1001GCN36SVCPP11ST) (V2) from Badger Meter, Inc. (Milwaukee, WI) was used. The upstream scHe pressure during coating experiments was controlled through a computer regulated PID control loop (F) by combining this pneumatic flow control valve with a high accuracy pressure transducer (±0.1 psi) (model PX01C0−7.5KG5T) (P) manufactured by Omega Engineering, Inc. The upstream scHe pressure fluctuation during coating can be maintained within ± 1 psi.

The drainage rate (or displacement velocity, U_w) during coating was controlled using a model 260D syringe pump (P2) manufactured by Isco, Inc. (Lincoln, NE). This pump can withstand pressures up to 7500 psi and can produce a maximum flow rate of about 100 mL/min at a given constant pressure. Supercritical CO_2 was supplied to the system by using a model 500D syringe pump from ISCO, Inc.(P1).

2.3. Deposition Methods and Procedures. All of the substrate coupons used in this study were first cleaned with acetone, methanol, and double distilled deionized water using a model 2510 Branson (Danbury, CT) ultrasonic cleaner. Right before deposition experiments, the substrate coupons were dried with nitrogen and placed on the substrate heating stage.

Prior to each deposition run, the temperature of the temperature control unit and the downstream ISCO pump was set at an experimentally desired value of 40 °C. The whole coating system including the upstream scHe line, the coating vessel, the downstream $scCO_2$ solution line and the downstream ISCO pump were purged with He at 300 psi for 10 min to remove solvent that may have been left after the system was cleaned. The coating vessel and the downstream line were then vented back to atmospheric pressure. The pressure of the upstream He line was maintained at 300 psi. The coating vessel was loaded with a known amount of $Cu(hfac)_2 \cdot H_2O$. The precleaned substrate was fixed to the substrate holder and loaded at the top of the coating vessel. After $Cu(hfac)_2 \cdot H_2O$ and the substrate were introduced in the coating vessel, the coating vessel was repurged with 100 psi of CO_2 for 10 min. The coating vessel was then filled with $scCO_2$ at a desired deposition pressure of 1800 psi. Extensive mixing using a magnetic bar and a magnetic stirrer at the bottom of the coating vessel was performed for at least 5 h. The downstream $scCO_2$ solution line and the downstream ISCO pump were repurged with 100 psi of CO_2 for 10 min and then pressurized with CO_2 at the same pressure as that of the coating vessel.

The deposition process consisted of several sequential steps. First, the coating vessel, the downstream $scCO_2$ solution line, and the downstream ISCO pump were pressurized with CO_2 at a desired pressure of 1800 psi. The upstream scHe line was pressurized with He at the same pressure as that of the coating vessel. The fluctuation of the pressure and temperature of the whole system were carefully monitored until the fluctuations were within ±1 psi and ±0.1 °C. After the pressure and temperature between the upstream scHe line, the coating vessel, and the downstream $scCO_2$ solution line were equilibrated, the upstream scHe isolation valve and the downstream $scCO_2$ solution isolation valve were opened. The deposition of $Cu(hfac)_2 \cdot H_2O$ on the substrate was then performed by displacing the $scCO_2$ solution phase with the upstream scHe phase using the downstream ISCO pump. The displacement velocity was adjusted by controlling the refilling speed of the syringe in the ISCO pump. After the $scCO_2$ solution was completely displaced with scHe and the Cu precursor was coated on the substrate, the coating vessel was isolated by closing the upstream scHe isolation valve and the downstream $scCO_2$ solution isolation valve. The coating vessel was then depressurized to atmospheric pressure over a 30 min time period. The long evacuation period was used to avoid any morphological changes that might be caused by fast evacuation. After He was evacuated from the coating vessel, hydrogen was introduced slowly into the coating vessel at a pressure of 600 psi. The reduction of the deposited Cu precursor film to Cu film was then initiated by increasing the temperature of the aluminum heating stage to 200 °C. The coating vessel wall temperature increased during reduction because of heat irradiation from the aluminum heating stage. For example, the coating vessel temperature at 5 min reduction period increased from 40 °C to ∼50 °C. At 60 min

reduction period, the coating vessel wall temperature increased to ~90 °C. At these coating vessel wall temperatures, Cu films do not form on the wall of the coating vessel but are only selectively deposited on the substrate.

The dependence of Cu particle size, film thickness and morphology on various coating conditions was investigated. Solution concentrations were varied from 0.5 to 3 wt % at a deposition pressure of 1800 psi and a displacement velocity of 0.0035 cm/s. All deposition of $Cu(hfac)_2 \cdot H_2O$ was performed at a temperature of 40 °C. The reduction periods were varied from 5 to 60 min at a fixed solution concentration of 3 wt % and a fixed displacement velocity of 0.0035 cm/s.

2.4. Characterization. The morphology of deposited Cu on the substrates was observed using A JEOL 6400F field emission scanning electron microscope (SEM). The accelerating voltage was 5 kV and the emission current was 8 μA. All the samples were mounted using a carbon tape on a custom built mount. Both top-view and cross-sectional view of SEM images on the same sample were collected. The cross-sectional views were taken by mounting the samples on a 30° tilted sample stage. The size of Cu particles was estimated by analyzing the top-view SEM images with Matrox Inspector, an image-processing program by Matrox Electronic Systems Ltd. (Quebec, Canada). An average diameter of particles was defined as the arithmetic average diameter of each hemispherical shaped particle in the SEM images. The average diameter of irregular shape particles was estimated with an assumption that their geometry is hemispherical.

X-ray photoelectron spectroscopy (XPS) measurements were carried out using a Riber LAS-3000 spectrometer with a hemispherical capacitor analyzer. An Mg Kα X-ray source was used to irradiate a 2−3 mm diameter spot on each sample at a voltage of 12 kV and an emission current of 15 mA. The pressure in the chamber was maintained below 1×10^{-7} torr during the measurement. All binding energies are referenced to the C 1*s* neutral carbon peak at 285.0 eV to compensate for surface charging effects. Data were collected at a takeoff angle of 75° between the sample and analyzer. Ar^+ sputtering was used to clean surface contaminants and to examine chemical species in the subsurface region of the substrates and the Cu films.

Secondary ion mass spectrometry (SIMS) analysis was performed using a CAMECA IMS-6f SIMS instrument. Cs^+ at 6 keV impact energy was used to bombard a 150 μm × 150 μm area of the Cu film. Secondary ions were collected from an optically gated 60 μm diameter area using the 150 μm contrast diaphragm and the 750 μm field aperture. The analyses were obtained at a mass resolution of $m/\Delta m = 1500$. The typical pressure in the instrument sample chamber was maintained at less than 1×10^{-10} Torr.

The film texture was characterized by X-ray diffraction (XRD) using a Scintag XDS 2000 X-ray diffractometer with a Cu Kα excitation source using 30 KV at 35 mA. A $\theta/2\theta$ geometry was used for all XRD analysis. Sample resistivity measurements were made using a Jandel four-point probe over approximately 1 cm × 1 cm areas.

3. Results and Discussion

3.1. Deposition of $Cu(hfac)_2 \cdot H_2O$ from Transient Interfacial Boundary between scHe and $scCO_2$. Immiscibility between supercritical helium (scHe) and supercritical carbon dioxide ($scCO_2$) only occur at extremely high pressure (for example, above ~ 22 000 psi at 40 °C and above ~ 117,600 psi at 80 °C).[51] However, at mild pressure (<6500 psi), $scCO_2$ and scHe were found to be transiently immiscible.[52] When a solute is dissolved in an $scCO_2$ phase and a scHe phase is introduced into the $scCO_2$ solution phase, the flux of He into the $scCO_2$ solution phase and the flux of CO_2 into the scHe phase can cause the solute to precipitate.[52,53] The flux of He and CO_2 between the scHe phase and the $scCO_2$ solution phase reduces solvent power of CO_2 at the interfacial boundary resulting in solution supersaturation and solute precipitation by a nucleation and growth mechanisms. Figure 2 shows an optical image of $Cu(hfac)_2 \cdot H_2O$ film deposited during displacement of a $scCO_2/Cu(hfac)_2 \cdot H_2O$ solution phase with scHe phase at a solution concentration of 1 wt%, a pressure of 1800 psi, a displacement velocity of 0.0035 cm/s, and 40 °C using the 18.3 mL coating vessel. It can be seen that branched $Cu(hfac)_2 \cdot H_2O$ crystal films were deposited on a silicon wafer substrate. Each crystal branch is roughly directed in the displacement direction. After the deposition of $Cu(hfac)_2 \cdot H_2O$ on the substrates, Cu particles and films were produced by reduction of the deposited film at a temperature of 200 °C with hydrogen.

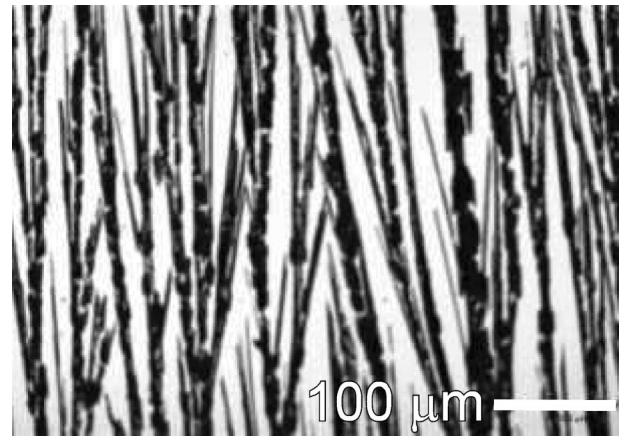

Figure 2. Optical microscope image of $Cu(hfac)_2 \cdot H_2O$ film deposited on silicon wafer substrate during displacement of the interfacial boundary at 1 wt%, 1800 psi, 0.0035 cm/s, and 40 °C.

3.2. Particle and Film Formation Mechanism of Cu from DISP. This section discusses Cu particle and film formation mechanism by examining reduction period effects on nucleation and growth of Cu. Figure 3a−e show top-views of scanning electron microscope (SEM) images of Cu deposited on SiO_x at various reduction periods ranging 5−60 min. Inset cross-sectional views of SEM images are shown in the upper right corner of each image. As shown in Figure 3a, isolated Cu nuclei particles with average diameter of 60 nm were produced on SiO_x during the 5 min reduction period. This indicates that the growth mechanism of Cu formed from the deposited $Cu(hfac)_2 \cdot H_2O$ is the Volmer−Weber island growth mode, i.e. the three-dimensional island growth mode.[54] It can be also seen that coalescence between nuclei created irregular shape particles (as indicated with the arrows in the image) with larger size (~80 nm). Coalescence between neighboring Cu nuclei was more activated during a 15 min reduction period, causing larger size particles with

(51) Tsiklis, D. S.; Rott, L. A. *Russ. Chem. Rev.* **1967**, *36*, 351.
(52) Kim, J.; Carbonell, R. G. *Langmuir* **2006**, *22*, 2117.
(53) Kim, J.; McClain, J. B.; Carbonell, R. G. *Langmuir* **2006**, *22*, 2117.
(54) Greene, J. E. Nucleation, film growth, and microstructural evolution. In *Handbook of Deposition Technologies for Films and Coatings*; Bunshah, R. F., Ed.; Noyes Publications: Park Ridge, NJ, 1994.

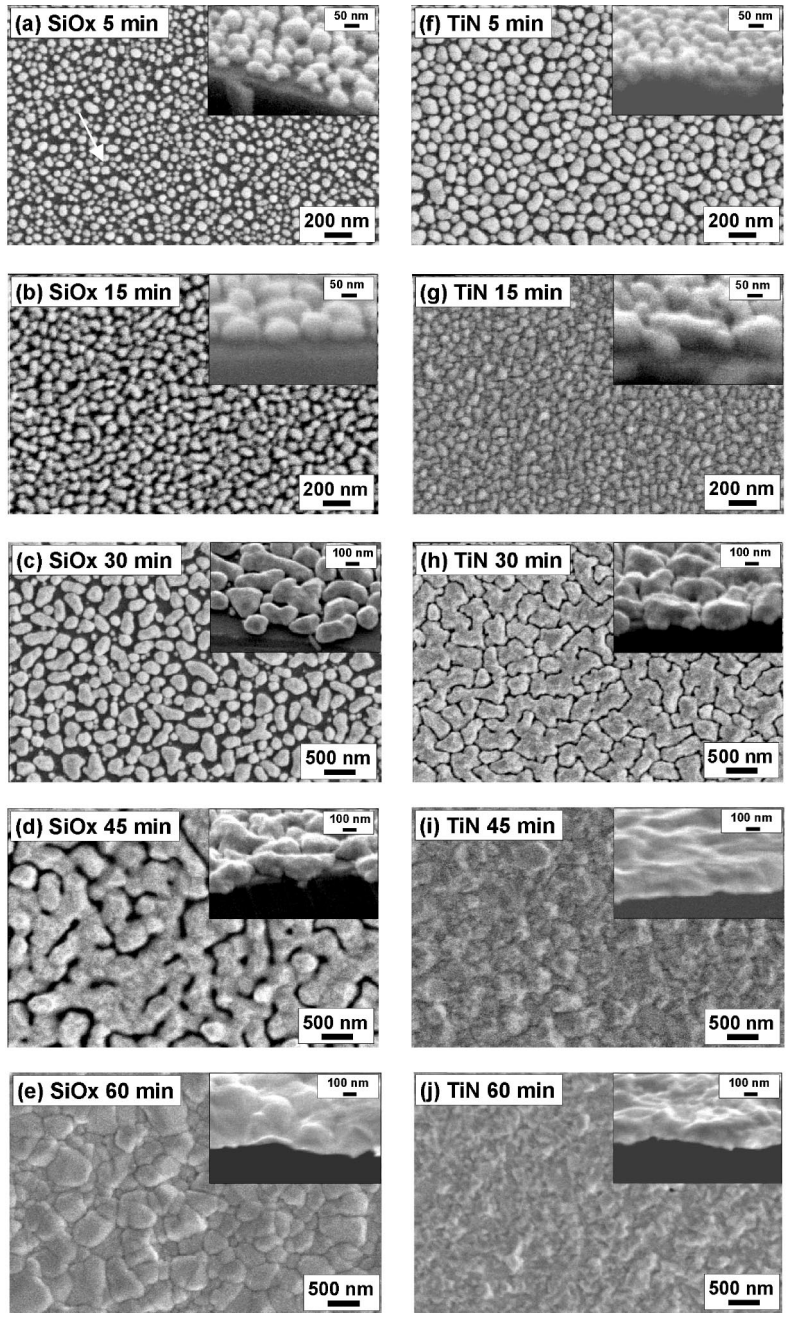

Figure 3. SEM images of Cu particles and films deposited on SiO_x and TiN at various reduction periods. $Cu(hfac)_2 \cdot xH_2O$ was deposited at a concentration of 3 wt%, at a fixed pressure of 1800 psi, at a fixed displacement velocity of 0.0035 cm/s, and 40 °C. The deposited Cu(II) compound films were then reduced at a H_2 pressure of 600 psi and a substrate heating stage temperature of 200 °C.

average diameters of 100 nm (Figure 3b). The particle size distribution is broad and the particles have various shapes. Further increases in reduction period to 30 min leads to linked island structure and larger size Cu particles with average diameter of 380 nm (Figure 3c). However, smaller particles with 40−50 nm in diameter and spherical shape are still observed. After a 45 min reduction time, well-connected film-like structure with significant amount of void (∼13%) resulted (Figure 3d). When the reduction period increased further to 60 min, complete coverage of the substrate by Cu films was obtained (Figure 3e). As shown in Figure S4 in the Supporting Information, low-magnification SEM images (× 10 000) revealed that deposition of uniform Cu films in a large area was possible using Cu DISP.

As shown in the Cu morphology changes with varying reduction period, the Cu film formation mechanism of Cu DISP is very similar to that of typical Cu CVD; three-dimensional nuclei formation, growth and coalescence of nuclei, and film formation.[6,55] The differences between Cu CVD and Cu DISP are (1) the initial stage of nucleation mechanism, and (2) continuous and batch operation process. First, the transport and adsorption steps associated with CVD are eliminated in Cu DISP. In a typical CVD process, Cu nuclei formation involves several sequential steps; gaseous organocopper compound molecules transport through a

(55) Kodas, T. T.; Hampden-Smith, M. J., Overview of metal C. V. D. In *The Chemistry of Metal CVD*; Kodas, T. T., Hampden-Smith, M. J., Eds.; VCH Publisher: New York, 1994.

boundary layer and adsorb on the surface of a substrate. Cu nuclei are formed by chemical reactions with or without a reducing agent at high temperature (>200 °C). Desorption of decomposed byproducts through the boundary layer to bulk gas mixture is necessary for the transition of Cu embryo into stable nuclei. In contrast, nucleation of Cu particles in Cu DISP only involves the chemical reaction of coated organocopper compound films and desorption of byproducts. As will be discussed later, the difference between the nucleation mechanism of Cu CVD and Cu DISP has very significant effects on initial nucleation behavior. Second, in Cu CVD, continuous feed of organocopper compound molecules to the surface of the substrate and continuous removal of decomposed byproducts from the surface of the substrate are necessary for three-dimensional island growth and film formation. In contrast, a batch process associated with Cu DISP does not allow continuous feed of organometallic molecules. DISP needs Cu precursor source inside of the coating vessel for further nuclei growth and film formation. The Cu precursor source is the precursor coated on the wall of the coating vessel. The coating vessel wall temperature increased continuously up to 90 °C during the 1 h reduction period. At this high temperature, the precursors coated on the wall of the coating vessel evaporated from the wall and reacted with the growing Cu particles on the substrate. This leads to the continuous growth of the Cu nuclei, coalescence between nuclei, and formation of the Cu film when the reduction period increases. In fact, it can be observed that $Cu(hfac)_2 \cdot H_2O$ was coated on the wall of the coating vessel at short reduction period regime whereas $Cu(hfac)_2 \cdot H_2O$ disappeared at long reduction period regime. Therefore, Cu film formation mechanism of DISP, deduced from the morphology changes with varying reduction period, is as follows; first, Cu nuclei are formed at short reduction time (~5 min) from the Cu precursor films coated on the substrate when the substrate temperature increased high enough for reduction reaction. These Cu nuclei act as a Cu seed layer for subsequent particle growth and film formation. The Cu films are then formed at long reduction time (45−60 min) from a "CVD-like" process by consuming the Cu precursor coated on the wall of the coating vessel.

3.3. Comparison of Reduction Period Effects of Cu on SiO_x and TiN. When TiN is used as a substrate, the reduction period effects on particle and film formation are different from those of Cu on SiO_x. Top-view and cross-section view of SEM images of Cu on TiN at various reduction period frames are cross-compared with those of Cu on SiO_x in Figure 3. When SiO_x was used as a substrate, nanosize Cu nuclei (40−60 nm in diameter) with spherical shape and larger size of coalesced nuclei (~80 nm in diameter) with irregular shape formed during the 5 min reduction period (Figure 3 (a)). The average diameter of Cu nuclei on SiO_x is 60 nm and the surface coverage of Cu on the substrate is ~80%. The number density of Cu nuclei on SiO_x was 1.87×10^{10} cm^{-2}. Initial Cu nuclei growth behavior on TiN is slightly different from that on SiO_x. As shown in Figure 3f, the average diameter (95 nm) and the surface coverage (~86%) of Cu nuclei on TiN produced at the same conditions are larger than those on SiO_x. It can be also seen that the size of Cu nuclei on TiN are irregular in shape and more widely distributed (40−250 nm in diameter) compared with the Cu nuclei on SiO_x. The difference in initial growth behavior is mainly due to faster formation of Cu nuclei and more active coalescence between neighboring Cu nuclei on TiN than on SiO_x. This results in a much smaller number density of the Cu nuclei (8.53×10^9 cm^{-2}) and larger surface coverage of Cu nuclei on TiN than those of Cu nuclei on SiO_x. At least three possible aspects are responsible for the difference in the initial nuclei growth behavior of Cu on SiO_x and Cu on TiN. First, the greater amount of electron density of the TiN substrate is favorable to destabilize the absorbed Cu(II) compound molecules in a more reactive state.[56,57] Second, the surface roughness of the TiN substrate, measured by AFM over a 1 μm × 1 μm scan area, is five times larger that that of SiO_x substrate (see the Supporting Information for details). Thus the TiN substrate offers more reactive nucleation sites such as kinks and steps.[58] Third, metallic-like TiN substrate can offer more thermodynamically favorable Cu nucleation and better Cu wetting.[59,60]

Although Cu DISP exhibits some degree of difference in the initial nucleation behavior with varying substrate, this difference is much smaller compared to the initial nucleation behavior of Cu CVD. Cu CVD nucleation is extremely sensitive to adsorption of organometallic molecules, chemical surface reaction and desorption of decomposed byproducts, which are in turn highly sensitive to surface properties of a substrate. Metallic surfaces with high electron density are more favorable to the adsorption of organocopper compounds in their activated state and the formation of Cu nuclei. Cu is not easily nucleated on nonmetallic surfaces because organometallic molecules tend to absorb in an intact state.[56] Thin oxide layer and impurities on metallic surfaces such as TiN, Ta, and Ti are known to have detrimental effects on Cu CVD nucleation.[61,62] This leads to undesirable film morphologies such as a discontinuous Cu film with significant amount of void or a Cu film with poorly connected grains. On the other hand, defects or scratches are known to enhance nucleation of Cu on nonmetallic surfaces such as SiO_2.[63] In addition, Cu CVD nucleation is also very sensitive to surface pretreatment, chemical composition, and physical roughness of surfaces.[58,64−67] In contrast, the nucleation of Cu DISP only involves chemical reaction of coated organocopper compound films and desorption of byproducts. Although some

(56) Cohen, S. L.; Liehr, M.; Kasi, S. *Appl. Phys. Lett.* **1992**, *60*, 1585.
(57) Cohen, S. L.; Liehr, M.; Kasi, S. *Appl. Phys. Lett.* **1992**, *60*, 50.
(58) Kroger, R.; Eizenberg, M.; Rabkin, E.; Cong, D.; Chen, L. *J. Appl. Phys.* **2000**, *88*, 1867.
(59) Jain, A.; Kodas, T. T.; Jairath, R.; Hampdensmith, M. J. *J. Vac. Sci. Technol., B* **1993**, *11*, 2107.
(60) Kim, D. H.; Wentorf, R. H.; Gill, W. N. *J. Vac. Sci. Technol., A* **1994**, *12*, 153.
(61) Kim, D. H.; Lee, Y. J.; Park, C. O.; Park, J. W.; Kim, J. J. *Chem. Eng. Commun.* **1996**, *153*, 307.
(62) Kim, D. H.; Wentorf, R. H.; Gill, W. N. *J. Appl. Phys.* **1993**, *74*, 5164.
(63) Kim, D. H.; Wentorf, R. H.; Gill, W. N. *J. Vac. Sci. Technol., A* **1994**, *12*, 153.
(64) Hu, M.; Noda, S.; Tsuji, Y.; Okubo, T.; Yamaguchi, Y.; Komiyama, H. *J. Vac. Sci. Technol., A* **2002**, *20*, 589.
(65) Lim, J. M.; Lee, C. M. *Solid-State Electron.* **2001**, *45*, 2083.
(66) Kroger, R.; Eizenberg, M.; Cong, D.; Yoshida, N.; Chen, L. Y.; Ramaswami, S.; Carl, D. *Microelectron. Eng.* **2000**, *50*, 375.
(67) Hong, L. S.; Lin, M. Z. *J. Appl. Phys., Part 2* **1997**, *36*, L711.

degree of difference in initial nucleation behavior between SiO_x and TiN was observed, Cu DISP nucleation is relatively insensitive to surface conditions compared with Cu CVD nucleation. As will be discussed later, similar degree of Cu nucleation was observed on low-*k* dielectric materials such as Silox, Coral, and JSR5190. The absence of an adsorption step and relatively high concentration of the organocopper molecules on the surface of substrates may be responsible for the insensitivity of Cu DISP nucleation to substrates.

When the reduction period increased to 15 min, a significant number of contacts between neighboring grains on TiN with a very small amount of void were observed (Figure 3g). The grain size is in the range of 80−150 nm in diameter and the thickness of each grain increased to ∼100 nm. The number density of Cu nuclei on TiN slightly increased to 9.28×10^9 cm^{-2} compared with that of the 5 min sample (8.53×10^9 cm^{-2}), suggesting that new Cu nuclei also formed between existing grains. In contrast, significant amount of void (∼20%) was observed in the Cu film on SiO_x after a 15 min reduction (Figure 3b). The thickness of Cu particles on SiO_x is smaller (∼65 nm) than the thickness of Cu on TiN at the same reduction period. Larger amount of void and thinner film on SiO_x relative to the film on TiN suggest that a smaller amount of Cu was deposited on SiO_x than on TiN. The number density of Cu nuclei on SiO_x decreased to 7.79×10^9 cm^{-2} compared with the sample at 5 min reduction period (1.87×10^{10} cm^{-2}). This indicates that two neighboring Cu nuclei coalesced and subsequent growth of Cu preferentially occurred on the surface of the existing Cu nuclei rather than initiating new nuclei on uncovered substrate when SiO_x was used as a substrate.

Figure 3h shows that well-connected Cu grains formed on TiN during 30 min reduction period. The grain size increased to ∼700 nm and the film thickness increased to ∼180 nm compared with the 15 min sample. However, the major characteristics of the 30 min sample is channellike void formation, an increase of the void distance between neighboring grains, and an increase in the amount of void compared with the previous 15 min sample. Migration and coalescence of neighboring grains may be responsible for the increase in grain size and new void formation. Smaller grains merged into larger grains and left a void at the former position.[68,69] In contrast, Cu produced on SiO_x during 30 min reduction period is comprised of isolated grains with highly irregular in shape and wide size distribution (Figure 3c). The size of large grains is in the range of 100−300 nm in diameter and the thickness is ∼130 nm. The number density of Cu particles decreased an order of magnitude to 8.86×10^8 cm^{-2} and the amount of void increased to 26% when compared with those of the 15 min sample. This may suggest that the main growth mechanism of Cu grain on SiO_x at this reduction time range is the migration−coalescence mechanism.

As shown Figure 3i, Cu film deposited on TiN after 45 min reduction completely covered the substrate. The grain size does not change much whereas film thickness increased to ∼220 nm when compared with the 30 min sample. This suggests that first Cu was deposited at the edges of grains, filling the gaps between grains and then further Cu deposition occurs on the surface of Cu films. In contrast, Cu film produced on SiO_x at the same reduction period retains a significant amount of void between grains (Figure 3d). The grains were well-connected and channel-like voids formed between the grains. The thickness of Cu on SiO_x increased from ∼130 nm to ∼180 nm when the reduction period increased from 30 to 45 min. However, this thickness is smaller than that of Cu on TiN at the same reduction period. Thus incomplete coverage and thinner thickness of the Cu film on SiO_x than those on TiN indicates less amount of Cu was deposited on SiO_x.

Figure 3j shows that Cu deposited on TiN after 60 min reduction period has less distinctive grain boundary compared with the 45 min sample. The film thickness is comparable to the thickness of the 45 min sample. This indicates that most of the Cu(II) compound in the coating vessel was consumed during the 45 min reduction period. Subsequent deposition from trace amounts of $Cu(hfac)_2 \cdot H_2O$ that was left after a 45 min reduction may occur on the grain boundaries of the Cu films during further reduction, resulting in very smooth and dense morphology. As shown in Figure 3e, most voids between grains were filled after a 60 min reduction period in the Cu film on SiO_x, resulting in almost complete coverage of the substrate. The thickness increased significantly to ∼450 nm compared with the 45 min sample on SiO_x. This film thickness is approximately two times larger than the film thickness of the Cu film on TiN (∼220 nm). Much thicker Cu films on SiO_x might be due to distinctive grain boundary or "microgaps" between grains. The Cu film on SiO_x has well-defined grains with broad size distribution of 100−700 nm and well-defined grain boundary. This morphology is very different from well-sintered and dense morphology of the Cu film on TiN. Therefore, the affinity of nucleation and lateral film growth of Cu on TiN may result in much denser Cu films on TiN compared with the film on SiO_x.

3.4. Cu Formation Dependence on Solution Concentration. Cu particle and film formation on SiO_x and TiN with varying $Cu(hfac)_2 \cdot H_2O$ solution concentration ranging 0.5−3 wt % at a fixed reduction period of 60 min were examined and SEM images are shown in Figure 4. At a low solution concentration of 0.5 wt %, Cu particles with almost identical size and shape formed both on SiO_x and TiN substrate (images a and e in Figure 4). The average particle diameter is 60 nm and the thickness is ∼40 nm, resulting in oval-like particle morphology. Size distribution of the Cu particles on (a) SiO_x and (b) TiN produced at 0.5 wt % were analyzed and shown in the Supporting Information. The nuclei densities (2.0×10^{10} cm^{-2}) and the size distribution of the Cu particle on both SiO_x and TiN are very similar. In both cases, particles in the range with 40−60 nm in diameter are the major populations (∼65%) and larger size particles with 80−90 nm in diameter are less than 2% of the total particles.

When $Cu(hfac)_2 \cdot H_2O$ concentration increased to 1 wt %, the morphology of Cu deposited on SiO_x is very different from those on TiN. As shown in Figure 4b, Cu produced on SiO_x has isolated island morphology with a significant

(68) Borgharkar, N. S.; Griffin, G. L.; Fan, H.; Maverick, A. W. *J. Electrochem. Soc.* **1999**, *146*, 1041.
(69) Shirakawa, H.; Komiyama, H. *J. Nanopart. Res.* **1999**, *1*, 17.

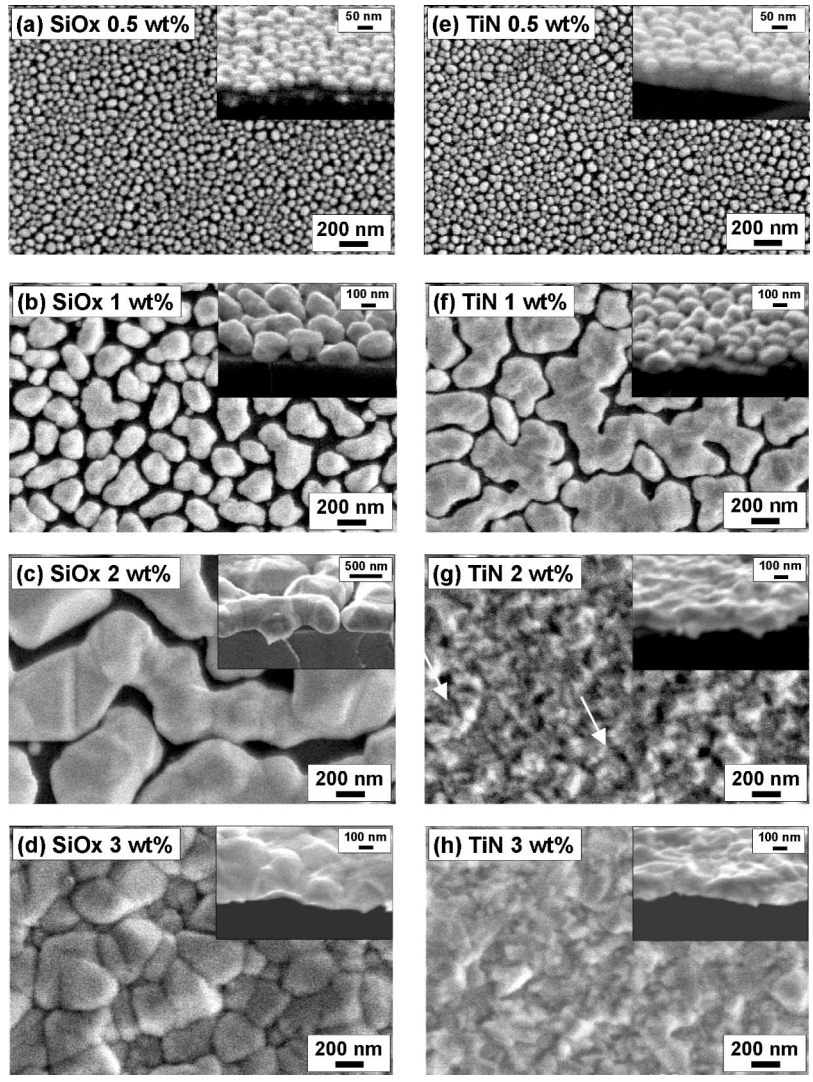

Figure 4. SEM images of Cu particles and films deposited on SiO_x and TiN at various $Cu(hfac)_2 \cdot xH_2O$ concentrations. $Cu(hfac)_2 \cdot xH_2O$ was deposited at concentrations of 0.5−3 wt %, at a fixed pressure of 1800 psi, a fixed displacement velocity of 0.0035 cm/s, and 40 °C. The deposited Cu(II) compound films were then reduced at a H_2 pressure of 600 psi, a substrate heating stage temperature of 200 °C, and a reduction period of 60 min.

Table 1. Nucleation Density, Particle (or grain) Size, Film Thickness of Cu Deposited at Various Reduction Periods[a]

	5 min		15 min		30 min		45 min		60 min	
	SiO_x	TiN	SiO_x	TiN	SiO_x	TiN	SiO*x*	TiN	SiO_x	TiN
nucleation density ($\times 10^{-9}$cm $^{-1}$)	18.7	8.53	7.79	9.28	0.886					
particle (grain) size (nm)	60	95	100	80 ∼ 150	100 ∼ 300	700		700	100−700	
film thickness (nm)			65	100	130	180	180	220	450	220

[a] $Cu(hfac)_2 \cdot xH_2O$ was deposited at a concentration of 3 wt %, at a fixed pressure of 1800 psi, a fixed displacement velocity of 0.0035 cm/s, and 40 °C. The deposited Cu(II) compound films were then reduced at a H_2 pressure of 600 psi and a substrate heating stage temperature of 200 °C.

amount of void between the grains. The grains are irregular in shape. The average grain diameter increased to 350 nm and the average grain thickness increased to 200 nm when compared with the 0.5 wt % sample. In addition, the grain density decreased by an order of magnitude (1.1×10^9 cm^{-2}) compared with the 0.5 wt % sample (2.0×10^{10} cm^{-2}). Again, this suggests that the main grain growth mechanism is coalescence of neighboring grains and subsequent Cu deposition occurs on the surface of existing Cu grains rather than on the uncovered substrate. The subsequent Cu was deposited via thermal reduction of the Cu precursors that were present inside of the reactor. In contrast, Cu on TiN produced at the same deposition conditions has well-connected grain structure with channel-like void between the grains (Figure 4f). As shown in cross-sectional images, the size of individual Cu grains on TiN is ∼200 nm and the thickness is ∼120 nm, which are smaller than those on SiO_x. This indicates that the higher electron density and rougher surface of TiN enhanced the lateral growth of Cu grains compared with the Cu growth on SiO_x.

Cu film on SiO_x reduced from $Cu(hfac)_2 \cdot H_2O$ coated at 2 wt % also has a different morphology from that on TiN. As shown in Figure 4c, Cu film with well-connected grain structure and channel-like voids between the grains resulted on SiO_x. In contrast, Cu deposited on TiN at the same conditions has almost a continuous film with isolated holes in the range of 80−100 nm in diameter (as indicated by the

Table 2. Nucleation Density, Particle (Or Grain) Size, Film Thickness of Cu Deposited at Various Reduction Continuous Cu Films Can Be Formed on Native Oxide of Silicon Substrate without Pretreatment of the Substrate or without Using Seed Layers[a]

	0.5 wt %		1 wt %		2 wt %		3 wt %	
	SiO_x	TiN	SiO_x	TiN	SiO_x	TiN	SiO_x	TiN
nucleation density ($\times 10^{-9}$cm^{-1})	20	20	1.1					
particle (grain) size (nm)	60	60	350	200				
film thickness (nm)	40	40	200	120	450	150	450	220

[a] $Cu(hfac)_2 \cdot xH_2O$ was deposited at concentrations of 0.5−3 wt %, a fixed pressure of 1800 psi, a fixed displacement velocity of 0.0035 cm/s, and 40 °C. The deposited Cu (II) compound films were then reduced at a H_2 pressure of 600 psi, a substrate heating stage temperature of 200 °C, and a reduction period of 60 min.

arrows in the SEM image) (Figure 4g). The film thickness of Cu on TiN slightly increased from ∼120 nm to ∼150 nm, whereas the film thickness of Cu on SiO_x significantly increased from ∼200 to ∼450 nm when the $Cu(hfac)_2 \cdot H_2O$ solution concentration increased from 1 to 2 wt %. Again, this suggests lateral growth of Cu on TiN was more enhanced compared with the Cu growth on SiO_x.

When the solution concentration increased to 3 wt %, almost complete coverage of Cu film on SiO_x was obtained (Figure 4d). The film thickness did not change much (∼450 nm) compared with the 2 wt % sample, indicating most of subsequent Cu nucleation occurs at the side edge surface of Cu grains. As shown in Figure 4h, the holes observed in the 2 wt % sample on TiN are completely filled in the Cu film produced at 3 wt %. The film thickness increased from 150 to 220 nm. Therefore, TiN is beneficial for lateral film growth, resulting in more dense Cu films at higher concentration.

3.5. Cu Deposition on various substrates. Cu films were deposited on tungsten (W), SiO_2 and low-*k* dielectric materials such as Silox, Coral, and JSR5109 coated wafer substrates and SEM images of the Cu films are shown in Figure 5. The coating conditions were Cu precursor concentration of 5 wt %, a displacement velocity of 0.055 cm/s, a CO_2 pressure of 1800 psi, and a temperature of 20 °C. The reduction conditions were a substrate temperature of 200−250 °C, a H_2 pressure of 80 psi and a reduction period of 5 min. The Cu film growth mechanism on SiO_2 and low-*k* dielectric materials appears to follow island formation under the deposition conditions based upon the SEM images as shown in Figure 5. Small, hemispherical grains are shown in the images, which are expected for the proposed growth mechanism. That is, the metal nuclei act to reduce their surface free energy and this is best accomplished by hemisphere formation. The Cu films adhered strongly to all substrates tested based on scratch and peel tests using pressure sensitive adhesive tape.

Cu films deposited from $Cu(hfac)_2 \cdot H_2O$ were specular in appearance with a Cu metal luster. Films deposited from copper(I/II) hexafluoropentanedionatevinyltrimethylsilane complex were cloudy and lacked the luster of Cu metal. Importantly, Cu films deposited from this precursor did not require addition of a reducing agent. This finding agrees with currently practiced industrial MOCVD deposition of Cu.[70] It also suggests that modeling of metal deposition using Cu DISP follows many of the same rules obeyed in conventional CVD. When the W substrate was used, Cu deposition temperature was 50 °C lower than the deposition temperature of SiO_2 or low-*k* dielectric materials. Most likely, the metal surfaces lower the activation energy required for the initial

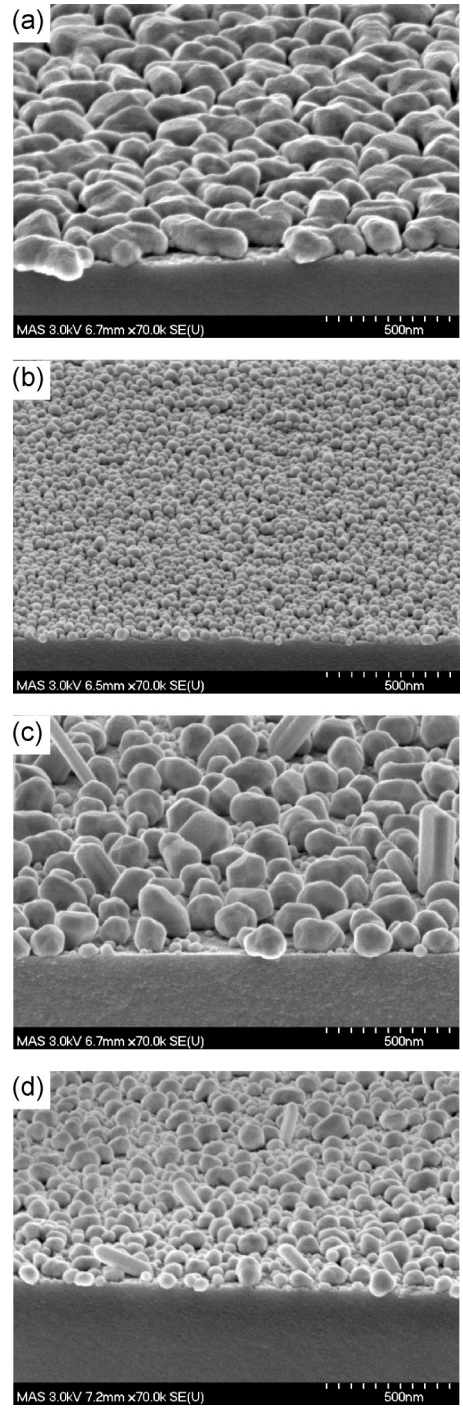

Figure 5. SEM images of Cu deposited on (a) SiO_2, (b) Silox, (c) Coral, and (d) JSR5901. $Cu(hfac)_2 \cdot xH_2O$ was deposited at a concentration of 5 wt %, a fixed pressure of 1800 psi, a fixed displacement velocity of 0.0055 cm/s, and 20 °C. The deposited Cu(II) compound films were then reduced at a H_2 pressure of 80 psi, a substrate heating stage temperature of 200−250 °C, and a reduction period of 5 min.

(70) Kodas, T. T.; Hampden-Smith, M. J., Eds.; *The Chemistry of Metal CVD*; VCH Publisher: New York, 1994; p 530.

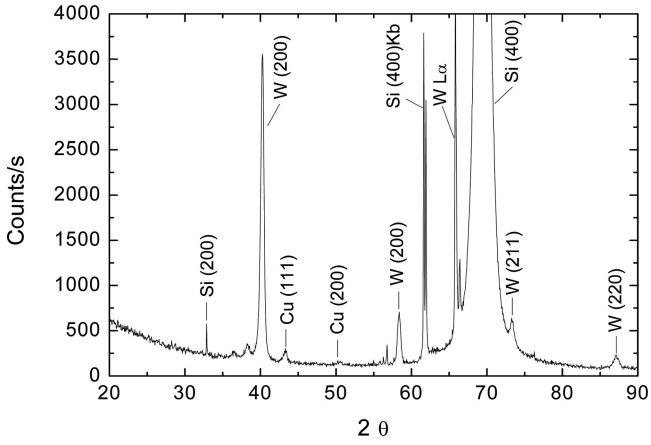

Figure 6. XRD of Cu film on W. $Cu(hfac)_2 \cdot xH_2O$ was deposited at a concentration of 5 wt %, a fixed pressure of 1800 psi, a fixed displacement velocity of 0.0055 cm/s, and 20 °C. The deposited Cu(II) compound films were then reduced at a H_2 pressure of 80 psi and a substrate heating stage temperature of 200−250 °C, and a reduction period of 5 min.

precursor adsorption event that is believed to occur when a soluble adsorption reaction byproduct is created.

Cu film resistivity measurements approached bulk Cu values when measured by standard four-point probe techniques. The resistivity measurements were carried out with the Cu films on the nonconducting substrates such as SiO_2, Silox, Coral, and JSR5109 coated wafer. Typical measured values for Cu films were 4 ± 2 $\mu\Omega$ cm compared to a bulk value of 1.7 $\mu\Omega$ cm and literature values of 1.8−3 $\mu\Omega$ cm^2 for CVD deposited Cu films. None of the Cu films were annealed prior to the resistivity measurement, which probably accounts for the difference between the experimentally measured and bulk resistivity values. The high resistivity of the DISP deposited Cu films on the nonconducting substrates can be also due to large grain size and poor connection between the grains. Alternatively, Cu film contamination by carbon and other impurities could produce higher resistivity than that of bulk Cu. This hypothesis will be supported by XPS analysis, as discussed in the following section. X-ray diffraction (XRD) analysis of the as deposited Cu film on W shown in Figure 6 indicates that it is polycrystalline with dominant (111) and (200) crystallographic orientations.

3.6. Chemical Composition Analysis of Cu film. The chemical composition of the Cu films was analyzed using XPS and secondary ion mass spectroscopy (SIMS). Figure 7a shows the XPS depth profile of the Cu film produced on TiN at the $Cu(hfac)_2 \cdot H_2O$ concentration of 3 wt % and at 60 min reduction period. Prior to sputtering, a considerable amount of carbon (18%), fluorine (12%), and oxygen (33%) contamination on the surface of the Cu film was observed. This was due to the nature of the DISP deposition process. Because supercritical CO_2 is absent during precursor reduction, limited opportunity exists for the removal of adsorbed reduction reaction byproducts. Mechanistic literature studies using surface vibrational spectroscopies of Cu deposition from copper β-diketonates such as copper(II) hexafluoroacetylacetonate show that hfac ligand species are surface bound even at temperatures of 250 °C under pressure

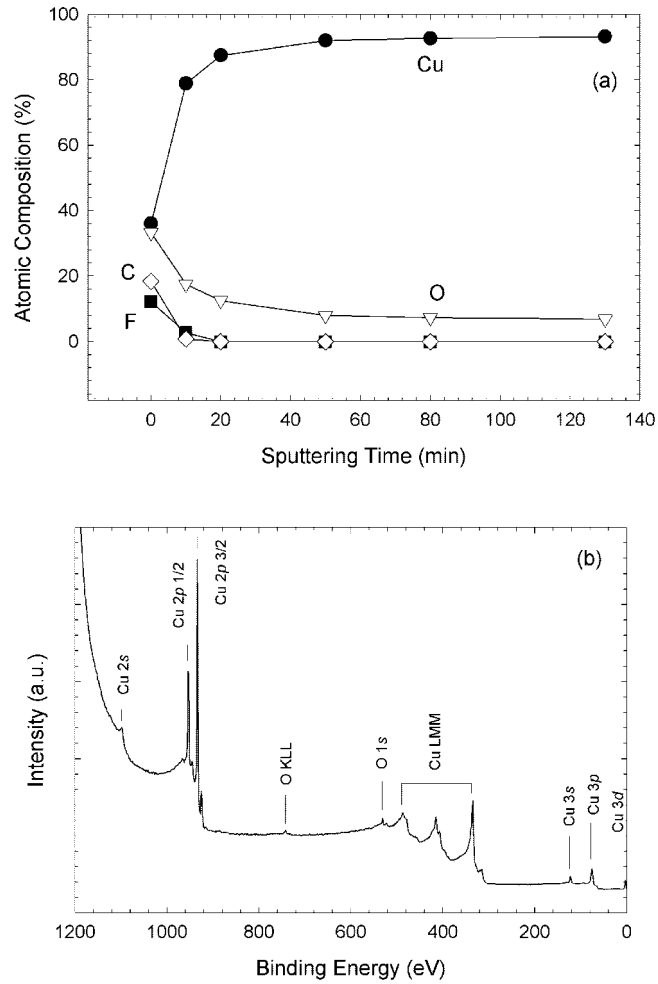

Figure 7. (a) XPS depth profile of the Cu film on TiN, and (b) XPS survey spectra after 140 min sputtering. $Cu(hfac)_2 \cdot H_2O$ was deposited at a concentration of 3 wt %, at a fixed pressure of 1800 psi, at a fixed displacement velocity of 0.0035 cm/s, and 40 °C. The deposited Cu(II) compound films were then reduced at a H_2 pressure of 600 psi, a substrate heating stage temperature of 200 °C, and a reduction period of 60 min.

conditions of a few millitorr.[71] After 20 min sputtering, fluorine and carbon peaks decreased below the detection limit of the instrument, whereas 8% of oxygen was still detected. Further sputtering does not remove oxygen completely. Figure 7b shows survey spectra of Cu on TiN after 140 min of sputtering. It can be seen that the O 1*s* peak at 530.1 eV and oxygen Auger peak at 742.9 eV persist. The oxygen composition is ∼ 7%. The secondary ion mass spectroscopy (SIMS) was employed to analyze chemical composition throughout the whole film and the result is shown in Figure 8. The oxygen concentration is largest at the interface between the Cu layer and the TiN layer, and then decreases in the TiN layer. This indicates that thin film of oxide layer was formed on the surface of the TiN substrate, which agrees well with the XPS spectra of the TiN substrate (as shown in the Supporting Information). The oxygen isotope 18 (O18) signal did not decrease below the noise to signal limit in the subsurface region of the film, suggesting the Cu film was oxidized. The maximum of the oxygen content at the interface between the Cu layer and the TiN layer was

(71) Girolami, G. S.; Jeffries, P. M.; Dubois, L. H. *J. Am. Chem. Soc.* **1993**, *115*, 1015.

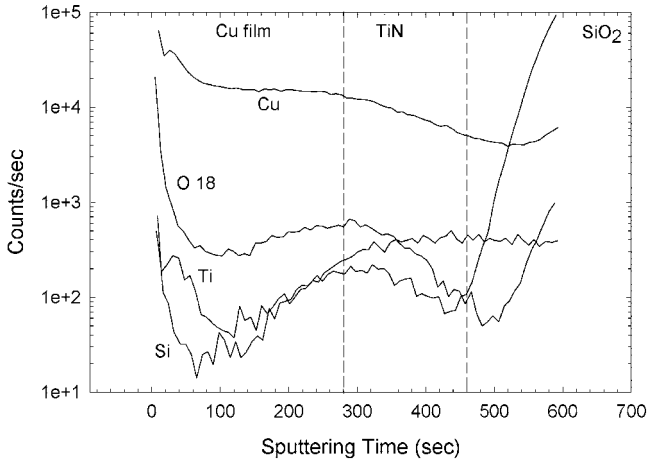

Figure 8. SIMS depth profile of the Cu film on TiN. $Cu(hfac)_2 \cdot xH_2O$ was deposited at a concentration of 3 wt %, at a fixed pressure of 1800 psi, at a fixed displacement velocity of 0.0035 cm/s, and 40 °C. The deposited Cu(II) compound films were then reduced at a H_2 pressure of 600 psi, a substrate heating stage temperature of 200 °C, and a reduction period of 60 min.

estimated to be approximately 6% atomic oxygen. This estimation was made on the basis of the O18 signal and an oxygen implant in silicon. The smaller oxygen content estimated from SIMS compared with the XPS result may be due to XPS instrumental artifacts. The XPS instrument and the Ar^+ sputtering unit were tested with a $\sim$ 20 Å thick native silicon oxide on a silicon wafer substrate. After 10 min sputtering, the native silicon oxide layer was successfully removed by the sputtering, confirmed by high-resolution spectra of Si 2p region. However, 6% oxygen was observed at a binding energy of 531 eV. Even after 120 min sputtering, $\sim$6% oxygen was detected. The oxygen in the subsurface region of the film may be due to an incorporation of oxygen during film deposition. Possible oxygen sources are water molecules in the hydrated Cu(II) compound and ambient oxygen in the coating vessel. Oxidation of the film during air exposure after film deposition may be also responsible for the oxygen incorporation because Cu films are easily oxidized in air.[72]

4. Conclusions

A new metal deposition process has been developed and Cu particles and films were produced on various substrates including SiO_x, TiN, W, and low-*k* materials such as Coral, JSR5109 and Silox. This process involves Cu precursor coatings from DISP followed by reduction in hydrogen. Cu particles in the range of 60−95 nm in average diameter formed at the lower precursor concentrations or at short reduction periods. Insensitivity of initial nucleation behavior to the surface properties of the substrates associated with Cu DISP makes it possible to produce Cu particles on low activity surfaces such as SiO_x and the low-*k* materials. Cu films in the range of 220−450 nm in thickness were produced on SiO_x and TiN at higher concentration and long reduction periods with a "CVD-like" mechanism. The XPS results showed that highly pure films with no carbon and fluorine incorporation in the subsurface region of the film were obtained. Because high-quality Cu particles and films can be produced on various substrates using Cu DISP, this process may be useful for Cu-based interconnect applications.

Acknowledgment. This work was supported by the STC Program of the National Science Foundation under Agreement No. CHE-9876674. Micell Technologies, Inc. acknowledges funding support of portions of this work from an Environmental Protection Agency SBIR Grant under Contract EP-D-04-042.

Supporting Information Available: AFM images of (a) the SiO_x substrate and (b) the TiN substrate; high-resolution spectra of the TiN substrate in the (a) C 1s, (b) F 1s, (c) Ti 2p, and (d) O 1s regions as a function of Ar^+ sputtering time; The nucleation density and the size distribution of Cu particles produced on (a) SiO_x and (b) TiN; low-magnification SEM images of the Cu films on SiO_x and TiN (PDF). This material is available free of charge via the Internet at http://pubs.acs.org.

CM802659J

(72) Li, J.; Mayer, J. W.; Colgan, E. G. *J. Appl. Phys.* **1991**, *70*, 2820.